Final, accepted version of:
Bakker, M. and Lane, S.N., 2017. Archival photogrammetric analysis of river-floodplain systems using Structure from Motion (SfM) methods. Earth Surface Processes and Landforms, 42, 1274-86
A typeset version is available at https://rdcu.be/biYFC

Earth Surface Processes and Landforms

Archival photogrammetric analysis of river-floodplain systems using Structure from Motion (SfM) methods

Journal:	*Earth Surface Processes and Landforms*
Manuscript ID	ESP-16-0224.R2
Wiley - Manuscript type:	Research Article
Date Submitted by the Author:	n/a
Complete List of Authors:	Bakker, Maarten; University of Lausanne, Institute of Earth Surface Dynamics, Lane, Stuart; University of Lausanne, Institute of Earth Surface Dynamics,
Keywords:	archival aerial imagery, classical photogrammetry, Structure from Motion (SfM) methods, systematic error minimisation, morphological interpretation

ABSTRACT

In this study we evaluate the extent to which accurate topographic data can be obtained by applying Structure from Motion (SfM) photogrammetric methods to archival imagery. Whilst SfM has proven valuable in photogrammetric applications using specially-acquired imagery (e.g. from unmanned aerial vehicles), it also has the potential to improve the precision of topographic data and the ease with which can be produced from historical imagery. We evaluate the application of SfM to a relatively extreme case, one of low relative relief: a braided river-floodplain system. We compared the bundle adjustments of SfM and classical photogrammetric methods, applied to eight dates. The SfM approach resulted in data quality similar to the classical approach, although the lens parameter values (e.g. focal length) recovered in the SfM process were not necessarily the same as their calibrated equivalents. Analysis showed that image texture and image overlap/configuration were critical drivers in the tie-point generation which impacted bundle adjustment quality. Working with archival imagery also illustrated the general need for the thorough understanding and careful application of (commercial) SfM software packages. As with classical methods, the propagation of (random) error in the estimation of lens and exterior orientation parameters using SfM methods may lead to inherent systematic error in the derived point clouds. We have shown that linear errors may be accounted for by point cloud registration based on a reference dataset, which is vital for the further application in quantitative morphological analyses when using archival imagery.

1. INTRODUCTION

Photogrammetry is a well-established technique that has been used to quantify morphologic change for many decades (e.g. Chandler and Moore 1989; Lane *et al.* 1993; 2000). In river-floodplain systems it has been applied to the investigation and monitoring of morphological change and sediment transport (Heritage *et al.* 1998; Chandler *et al.* 2002; Brasington *et al.* 2003; Lane *et al.* 2010; Wheaton *et al.* 2010; 2013), river bank erosion (Barker *et al.* 1997; Pyle *et al.* 1997; De Rose and Basher 2011), flood risk assessment (Sanyal and Lu 2004; Saint-Geours *et al.* 2015), river restoration and ecology (Gilvear *et al.* 1995; Kondolf and Larson 1995; Pasquale *et al.* 2011; Dietrich 2016), and archaeology (Perez, 2013). For the investigation of morphological change, particularly in braided river systems, a thorough theoretical and practical basis has been developed, including the assessment of error and uncertainties (Lane *et al.* 2003; Westaway *et al.* 2003; Lane *et al.* 2004; Wheaton *et al.* 2010).

The application of archival photogrammetry for the investigation of historical river evolution has been limited to a few studies, typically at the annual scale (Lane *et al.* 2010; Wheaton *et al.* 2010; 2013). Critical for such application is the scale and frequency of available imagery which determine the potential for detecting and quantifying morphological change (Gilvear and Bryant 2005). First, observed changes in river-floodplain systems are typically of the order of decimetres to meters, close to the limits of detection as predefined by image scale (Lane *et al.* 2010). This makes error identification and correction particularly important (Lane *et al.* 2004) and calls for cautious error propagation that is not overly conservative in terms of rejecting small magnitude but spatially coherent changes (Wheaton *et al.* 2010). Second, as the time between available surveys increases, so does the probability of intervening erosion and deposition, which may significantly impact upon the cumulative volumes of change detected (Lane *et al.* 1994).

Most recently, Structure from Motion (SfM) photogrammetry (Snavely 2008; Westoby *et al.* 2012; Smith *et al.* 2015) has been advocated as allowing a more efficient generation of precise and high-density point cloud data as shown for river bed geomorphology (e.g. Fonstad *et al.* 2013; Javernick *et al.* 2014). SfM methods also have appeal because they use computer vision techniques to assist with the interior and exterior orientation of imagery: (a) substantially reducing the need for user involvement, and so further automating the photogrammetric process; and (b) using much more of the information contained within the imagery to aid the orientation process so, in theory, improving the quality of the analysis. This approach may therefore unlock large historical photogrammetric archives for morphologic analysis. However, the algorithms upon which the SfM software is based are often undisclosed, particularly in commercial packages, and vary in the ability of the user to asses and control the estimation of exterior orientation parameters as compared with classical methods (e.g. Smith *et al.* 2015; Eltner *et al.* 2016), particularly concerning lens modelling (James and Robson 2014; Eltner and Schneider 2015). This is particularly relevant because Lane *et al.* (2004) showed that random error in estimated exterior orientation parameters can propagate into systematic error in a DEM, which may be in the order of decimeters or more. Such errors become apparent for the DEMs of Differences (DoDs) of river-floodplain systems where detected changes are small and a tilt or banding effect may appear (e.g. Stojic *et al.* 1998; Westaway *et al.* 2003; Lane *et al.* 2004). Systematic errors may be even larger when exterior orientation parameters are not reliably estimated due to poorly distributed Ground Control Points (GCPs) (e.g. James and Robson 2012; Bertin *et al.*

2015; Honkavaara *et al.* 2016). Thus, systematic errors resulting from photogrammetric reconstruction may have substantial impacts upon estimates of volume change and subsequent geomorphic interpretation.

The aim of this paper is to evaluate the application of SfM methods to archival imagery, specifically for the quantification of morphological change at the decadal scale in a river-floodplain system, so as to identify wider lessons for the application of these methods in geomorphic studies in general. We do this in three ways. First, we evaluate SfM bundle adjustment results and compared these with classical photogrammetric and camera calibration data. Second, we identify the controls on the (potential) quality of SfM results to assist in the identification of suitable archival imagery. Third, we address systematic errors that are inherent to both the classical and SfM photogrammetric approach and illustrate their potential impact on morphological interpretation if they are not adequately treated. This work is undertaken using a case-study: a braided river section of the Borgne d'Arolla in south-west Switzerland.

2. METHODS

2.1 Overview

The methodological approach is based on the application of SfM photogrammetry to archival river imagery and subsequent evaluation of the bundle adjustment parameters through comparison with classical photogrammetry and available camera calibration data. We used Pix4D, a commercially-available software package, for a Ground Control Point (GCP) assisted bundle adjustment and georeferencing of scanned historical images. This resulted in eight topographic data sets spanning the period 1959-2005. The focus of the subsequent analysis was threefold. First, we evaluated the accuracy of the bundle adjustment and compared: (a) the SfM-estimated exterior orientation parameters with values derived using a classical photogrammetric approach; and (b) SfM-estimated lens parameters with the parameter values in the associated camera calibration certificates. Second, we assessed image acquisition properties (e.g. image texture, overlap) that impact on the (potential) quality of the SfM bundle adjustment and the resulting point cloud precision and accuracy. Third, we considered the extent and nature of residual systematic errors in the photogrammetrically-generated point clouds and minimized these by means of registering stable zones to a reference dataset.

2.2 Case study: Borgne d'Arolla

The Borgne d'Arolla is a tributary of the Upper Rhône draining the Pennine Alps in south-west Switzerland. Under normal flow conditions, all water is abstracted by intakes at the tributary headwaters for the generation of hydropower (Gurnell 1983; Bezinge *et al.* 1989). This enables the application of photogrammetry on a more or less dry riverbed in the upstream reaches, without requiring correction procedures associated with under water topography (Westaway *et al.* 2001; Lane *et al.* 2010). This study is motivated by the aim of using archival photogrammetry to study the morphological evolution of four braided river reaches (Figure 1; for the purpose here, we will refer to reaches C and D as the combined reach CD) since the onset of hydropower exploitation in the early 1960s.

2.3 Archival aerial photographs

Historical aerial photographs were acquired from the Federal Office of Topography (SwissTopo) for the period 1959-2005 (Table 1). The images are black and white with the exception of 1999 and 2005 which are in colour. The image scale is in the range of 1:19000 - 1:27000 and they were scanned at a resolution of 14 or 21 μm by SwissTopo (original images were not available for higher resolution scanning). The images were acquired with large format photogrammetric cameras, came with camera calibration certificates (available online: http://www.swisstopo.admin.ch) and camera position data was available for images from 1983, 1995, 1999 and 2005. In addition to these images, an aerial lidar-based 2 m resolution DEM (ALTI3D), filtered for vegetation and buildings, was available from SwissTopo for the year 2010.

As archival imagery can be of variable quality and can be acquired using different image configurations, we aimed to characterise these using two (derived) properties (Table 1). First, we determined the texture of the resulting orthoimage using an entropy measure:

$$e = \sum_{i=1}^{I} p(i) \log_2 p(i) \qquad [1]$$

where I is the number of intensity levels on an 8 bit grey-scale image; and $p(i)$ is the probability density function of the image intensity (Gonzalez *et al.* 2003). The calculation of e was restricted to the river reaches and a 150 m buffer around them. Second, we determined the extent of image overlap as the fraction of the stereo-matched area (minimum of 2-3 overlapping images required) with respect to the total available image area. We assess the effects of these image acquisition properties on the bundle adjustment quality.

2.4 Ground control

Ground Control Points (GCPs) of fixed objects, houses, boulders etc. were surveyed with dGPS (see Micheletti *et al.* 2015) along the bottom and eastern side of the valley

(Figure 1). Although they cover the region of interest, they are not ideally distributed over the extent of the used photographs. Due to the difficulty in identifying stable points over the studied time period, GCPs are scarce in steeper terrain that is either heavily vegetated or unstable. As part of the methodology, additional zones were sought that were likely to be stable during the study period, i.e. without vegetation and human impacts (Figure 1). These were selected along the valley bottom and manually digitized based on orthoimages, where an optimal trade-off was sought between surface area, distribution and presumed stability.

2.5 Photogrammetric analysis

Photogrammetric data analysis of the sets of historical images (Table 1) drew upon two different sets of methods. As a starting point we use analyses conducted by Regamey (2013) with the classical photogrammetric ERDAS Imagine Leica Photogrammetry Suite (LPS) 2010. Classical airborne photogrammetry typically proceeds by: (1) image delineation and reconstituting lens parameters, aided by camera calibration certificates; (2) using initial estimates of (relative) camera position and orientation, GCPs and automatically generated tie-points between overlapping images to estimate the position and orientation of the camera during image acquisition: the bundle adjustment; and (3) applying stereo-matching to extract 3D point clouds. A detailed account on the application of this procedure in an Alpine landscape, including applied triangulation parameters/constraints and Automatic Terrain Extraction (ATE) correlation parameters, is given by Micheletti *et al*. 2015. We compare the bundle adjustment results with the SfM-based photogrammetric approach applied in this study.

SfM has become a well-established method in geomorphology that refers to a wide range of computer vision techniques, which have been applied to photogrammetry (see Smith *et al.* 2015 for review). Here, we use the software Pix4D that has been previously been applied in geomorphological studies by Castillo *et al.* (2014) and Eltner *et al.* (2015). The basic difference with classical photogrammetry is that the analysis commences with the application of automatic stereo-matching algorithms using computer vision techniques to an unstructured set of images. This forms the basis for bundle adjustment, hence (largely) automating steps 1 and 2 in the classical photogrammetric approach described above. This process provides a large dataset of tie-points and this redundance in theory eliminates the need and dependency on *a priori* specified: (a) image extent, in the form of fiducial marks; and (b) lens parameters, i.e. focal length, principle point of autocollimation and distortion (e.g. Vallet *et al.* 2011; Aguilar *et al.* 2013); in the determination of (c) exterior orientation parameters (e.g. Küng *et al.* 2011). SfM typically doesn't require or even support the input of GCPs, although they may be used to aid the determination of exterior orientation parameters *a priori*, or to scale, to rotate and to translate the resulting point clouds *a posteriori* (e.g. Javernick *et al.* 2014; Nebiker *et al.* 2014). Whilst early geomorphological application of SfM was hailed as freeing the user from the required expertise and time associated with classical photogrammetry (e.g. Fonstad *et al.* 2013), subsequent research indicates that most if not all of the well-established photogrammetric controls on data quality remain. Amongst others, Wackrow *et al.* (2007), Wackrow and Chandler (2008) and James and Robson (2014) showed that non-linear systematic errors may occur where self-calibration algorithms, on which SfM applications rely, are limited in resolving lens distortion, particularly for near-nadir acquired imagery typical in archival photogrammetry. This may be minimized through the use of GCPs in the bundle adjustment (Eltner and Schneider 2015), which is possible in Pix4D and for which purpose we used all GCPs in this study.

We used the original scanned aerial photographs in Pix4D v2.0 with large-frame extension. There was no need to downscale for processing time (e.g. Westoby *et al.* 2012; Caduff and Rieke-Zapp 2014) or to perform preliminary masking of the instrument strip and edges (Gomez *et al.* 2015). Although Pix4D allows the *a priori* specification of interior orientation parameters, we chose to specify only the initial (calibrated) focal length and allowed the use of self-calibration for the optimization of the bundle adjustment (note that in some SfM packages camera parameters may not be specified and self-calibration is applied automatically). This reflects the often-expressed rationale of SfM (e.g. Fonstad *et al.* 2013) that it facilitates the use of uncalibrated cameras or ones where lens parameters are not known. Then, we assessed the potential limitations of SfM-based camera self-calibration with archival imagery by using the measured distortion in the calibration certificate and the statistical fit from ERDAS that was based on this. Lens distortion is typically modelled after Brown (1971):

$$\begin{pmatrix}\Delta x\\ \Delta y\end{pmatrix} = \begin{pmatrix}(1+K_1r^2+K_2r^4+K_3r^6)x+2P_1xy+P_2(r^2+2x^2)\\ (1+K_1r^2+K_2r^4+K_3r^6)y+2P_2xy+P_1(r^2+2y^2)\end{pmatrix} \qquad [2]$$

where $\Delta x, \Delta y$ are the deviations of coordinates x, y due to distortion, $r^2 = x^2 + y^2$, K_1, K_2, K_3 and P_1, P_2 are the radial and tangential lens distortion parameters respectively. This forms the basis for both the ERDAS Imagine LPS and Pix4D models, where in ERDAS a linear K_0 term is introduced (instead of the 1), which is not required in numerical applications (e.g. Luhmann *et al.* 2014), and $K_3 = 0$ (ERDAS Imagine 2009). In Pix4D the distortion terms are presented in terms of R_x, T_x where $R_x = K_x f^{2x+1}$ (Pix4D 2016).

During initial processing in Pix4D, a binary descriptor of the SIFT (Scale Invariant Feature Transform) algorithm (Lowe 2004), similar to Strecha *et al.* (2012), is used to extract and then to match features from photographs (Küng *et al.* 2011). Based on these and GCP data, Pix4D performs an iterative routine of camera self-calibration, Automatic Aerial Triangulation (AAT) and Block Bundle Adjustment (BBA) to determine and to optimize interior and exterior parameters. The exact sequence of processes and the optimization approach, i.e. cost functions used to assess the calculated reprojection errors (Triggs *et al.* 1999) are proprietary and not disclosed. After initial processing, maximum point cloud densification is performed, based on Multi-View Stereo (MVS) algorithms (Seitz *et al.* 2006), and orthoimages and DEMs are generated. We visually verified whether the automatically generated DEM's showed non-linear or dome-like systematic errors, using the 2010 ALTI3D as reference, before we used the densified point cloud for registration and final DEM generation.

We initially evaluate the bundle adjustment results using the typical performance indicators, average reprojection error and root mean square error (RMSE), which are based on the distance between the matched tie-point and/or marked GCP and its modelled position on the image. In addition, we compare the estimated exterior parameters, camera position X, Y, Z in the Swiss coordinate system CH1903, and orientation yaw (K), pitch (ϴ) and roll (Φ), with values derived from classical photogrammetry (Regamey 2013) and camera position data (SwissTopo). To facilitate comparison amongst the parameters, the values of the orientation parameters were translated to a potential error they may induce in planform position (in the case of K) and elevation (in the case of ϴ, Φ) for a 1 km reach with a mean error of zero. We also compared the SfM estimated radial distortion (based on equation 2) with camera calibration certificates and values derived using ERDAS Imagine LPS.

2.6 Point cloud registration

As it has been shown that (random) error in exterior orientation parameters can propagate into systematic linear error in DEM surfaces (Lane *et al.* 2004), we aimed to correct and to assess this effect through registering the photogrammetrically acquired point clouds to the 2010 Lidar-based ALTI3D reference grid (SwissTopo). The potential of such an approach has already been demonstrated by Habib *et al.* (2004) and applied to archival photogrammetry by Miller *et al.* (2008) and Lane *et al.* (2016). Here, we used Riscan PRO software, which has its origin in the processing of terrestrial laser scanner point clouds (e.g. Heritage and Hetherington 2007; Heritage *et al.* 2009), and applied multi-station adjustment (e.g. Gabbud *et al.* 2015) to the point cloud data from Pix4D and the reference grid.

The adjustment is based on so-called plane patches, which were derived from stable zones within the point clouds (Figure 1). In a filter routine, the planes are defined where a minimum of 3 points can be aligned within a 2 cm standard deviation (normal distance between points and plane). This is done for successively smaller grids ranging from 32.768 m to a minimum of 0.128 m (Riegl 2015). A least-squares point matching algorithm (Zhang 1994), was then used to iteratively identify the translation and rotation parameters (scaling was not applied) needed to minimize the error between the stable patches for different years with respect to the reference grid. For this a search radius of 2 meters was used, equal to the size of the reference grid. We assessed the resulting reduction in (mean) error and compared the necessary adjustments amongst the reaches and with respect to the differences found in exterior orientation parameters between the SfM and classical approach.

2.7 DEM and DoD generation

To generate collocated 1 m resolution DEM grids, we applied a (default) linear point kriging variogram (slope and anisotropy equal to 1) to the resulting point clouds using Surfer 10 software (e.g. Heritage *et al.* 2009). DEMs of Differences (DoDs) were determined for consecutive periods and clipped to the maximum extent of the active river bed which was manually digitized from the orthoimages, excluding areas where construction took place. This allowed us to assess the effect of the registration adjustment and its potential impact on morphological interpretation.

3. RESULTS

3.1 Quality of the SfM bundle adjustment

Table 2 shows the number of GCPs and the number of extracted and matched tie-points used in bundle adjustment. The reprojection error of these points is within 10 cm and the resulting mean RMSE values between ±0.20 and ±0.45 m, both of which are in the same order of magnitude as values derived using classical photogrammetric methods (Regamey 2013). Table 3 relates the control point RMSE, reflecting the attained precision of bundle adjustment, to the theoretical precision which may be estimated by the object space pixel size derived from the image scale and scanning resolution (Lane *et al.* 2003). In general, the RMSE values are comparable, but when we resolve the mean and standard deviation of error in the SfM derived data, residual errors are revealed. Mean error over the whole study area is generally within the order of 5 cm, but higher values of up to 20 cm are found (Table 3). This suggests that there may be systematic error in the DEM surface, indicating the importance of subsequent point cloud registration.

3.2 Exterior orientation and lens parameter estimation

In addition to the assessment of bundle adjustment quality, we compared the constituent exterior orientation parameters that were derived from SfM and classical bundle adjustment (Table 4). In general, there is a good agreement in the planar positioning of the images: with one exception these were all within 10 meters. A slight systematic offset is detected in the X and to a lesser extent Y values. Larger differences are found in flying altitude, in the case of 2005 more than 25 meters. However, these differences are largely attributable to the focal length adjustment that occurred during lens parameter optimization in SfM processing (significant relation in Figure 2). We verified this by fixing the lens parameters for 2005, which resulted in a marked reduction in altitude difference to about 6 meters (last row Table 4). The resulting reprojection error and RMSE however increased to 0.20 and ±0.73 m respectively. Thus, there is evidence that the SfM approach, at least for a large part, compensates between estimates of exterior orientation parameters and those of lens parameters.

Regarding camera orientation, considerable differences in the yaw (Κ) are found, which may be related to the distribution of GCPs and the limited number of tie-points in the classical approach (Table 4). Pitch (Θ) and roll (Φ) values show a good agreement with the values derived using classical photogrammetry provided that they are not required to 'accommodate' larger deviations in lens parameters. Note the decrease in difference when using a fixed focal length in 2005. The differences in orientation appear to compensate for the effects of the adjusted focal length, at least partially, but potentially also the lens distortion.

Figure 3 illustrates the results of camera self-calibration in Pix4D compared to the measured distortion from the camera calibration certificate and the statistical fit from ERDAS based on these measured values. It is clear that the form of the polynomial form is not recovered, something which we find for other years in the dataset. However, the absolute lens distortion and the deviation from the calibrated distortion curve is very small, a few μm. The terrain displacement associated with this is less than 0.10 m and therefore much smaller than the pixel resolution of 0.35 m on which the self-calibration operates. For all years we found that the modelled absolute radial and tangential distortion didn't exceed the measured distortion which was maximally 8 μm. Resulting differences will therefore have no major impact on the exterior orientation parameters (Table 4) or the quality of the bundle adjustment (Table 2).

3.3 Impacts of image acquisition parameters

Figure 4 shows the relationship between image acquisition properties and bundle adjustment quality. It should be mentioned that the bundle adjustment quality defines the best achievable or potential error, that is without additional errors associated with stereo-matching. The ability of SfM to extract and match tie-points is clearly related to entropy (the same may be expected for classical photogrammetric packages), emphasizing the importance of image texture. The extent of image overlap also appears to affect the ability to retrieve tie-points, but through a non-linear relation which may reflect a minimum threshold that is required for the successful matching of tie-points. The influences of image texture and overlap on the number of tie-points works through in the reprojection error and RMSE values, although it is slightly modulated (Figure 4). The low number of tie-points in 1965 and to a lesser extent 2005, has limited repercussions on the reprojection error and RMSE. This may indicate the importance of GCP's which are used in the bundle adjustment and insure a base level quality – although marking these also requires sufficient texture. The number of applied images alone is not of critical importance, but more their configuration and the resulting overlap. Whereas the overlap correlation values are highest and most significant, entropy may be of even larger importance when the 1965 outlier is disregarded, which results in less scattered and markedly steeper (linear) relations. Finally, we find that the scale, with which we assessed the theoretical precision of the bundle adjustment, has no significant effect on the tie-point generation or reprojection error, but shows a significant increasing trend with the resulting RMSE (again 1965 is an outlier). It seems to limit the potential accuracy and precision that may be obtained, but does not directly control the bundle adjustment or is decisive for its quality, particularly in comparison with image texture and overlap.

3.4 Systematic error minimization in SfM point clouds

Where the mean error may average out to be more or less negligible on the scale of the entire study area, errors due to the incorrect DEM positioning or orientation may be large at the smaller reach scale. This is illustrated in the clear bias shown in the DoD in Figure 5b, where the 2005 DEM lies systematically below the reference 2010 Alti3D. Figure 5c shows the same DoD where the DEM was registered based on the surrounding stable area (Figure 5a). Through applying registration, the bias is nearly completely removed, the absolute mean error decreases from 0.52 to 0.03 m and a nearly symmetric distribution of residuals is obtained (Figure 6). In addition, the standard deviation is slightly reduced from ±0.66 m to ±0.56 m, which will also allow a better limit of detection when analyzing morphological change. Note that these values are not reflected in the mean error (0.02 m) and standard deviation (±0.21 m) of the entire study area as determined in the bundle adjustment (Table 3), emphasizing that the latter is not a sufficient indicator of the quality of derived DEMs which requires an independent reference dataset.

Table 5 summarizes the mean error per reach before and after registration. On the whole, the decrease in absolute error is in the order of centimeters to tens of centimeters. Where there are consecutive and opposite errors such as 1959 and 1965 in reach B this can lead to an increased DoD error, 0.86 m as opposed to 0.08 m after error minimization. However, the adjustment is not always as effective (e.g. reaches B and CD in 1983) where the residual systematic error remains more or less intact. The improvement due to registration can also vary significantly between different reaches for the same year, e.g. 1959 and 1995 and between years, e.g. reach CD in 1977 and 1983. These indicate that, despite visual inspection, residual non-linear structural errors may still be present. However, with two exceptions all of the residual mean error values are within ±15 cm.

To gain insight into the nature of the registration we compare the reaches amongst each other and relate them to the differences found between SfM and classical photogrammetric bundle adjustment. The individual registration adjustments of the different reaches show a general level of consistency but may also vary significantly per year (Figure 7). The translational shifts in X and Y show a somewhat similar but opposite pattern as the difference between SfM and classical photogrammetry and could partially compensate for this. The changes in Z values are relatively consistent between the reaches and smaller than the residual difference found for the bundle adjustment, we corrected for height difference due to focal length using the relation in

Figure 2, giving us confidence in the quality of the SfM derived altitudes. The required adjustment in yaw (K) is small when compared to the bundle adjustment differences, which is supported by the notion that the large number of image-covering tie-points in SfM photogrammetry enable more accurate image alignment. Adjustments in roll (Φ) are considerable and show a similar behavior as the differences in bundle adjustment. Rather than diminishing these differences they appear to correct for a common error. In this orientation, valley perpendicular, the bundle adjustment is not well constrained by the GCPs, as opposed to the valley parallel orientation where differences in pitch (Θ) adjustment are small. The magnitude of change in the exterior orientation parameters (Figure 7) with respect to the resulting decrease in error (Table 5) may give additional insight into the effectiveness of the registration and quality of the results. A relatively large decrease in error was achieved in reach B and CD in 2005 with a relatively limited adjustment in parameters; a shift in X and Z for reach B, and adjustment in roll (Φ) and to a lesser extent Z for reach CD. This gives confidence that a linear systematic error has been effectively corrected, moreover because little error is expected from potential instability of presumed stable areas with the reference year 2010. However, relatively large changes over a number of orientation parameters do not necessarily lead to significantly better results, for instance reaches B and CD in 1983, and these adjustments must be taken with caution. This may indicate an attempt to fit the data to non-linear or random error, potentially introducing (additional) systematic error.

Figure 8 shows the volumetric changes of the reaches through time, before and after registration adjustment, the latter including a correction for residual stable-zone mean error. Based on the available images and applied setting, we can conclude that volume changes due to systematic errors are of the same order of magnitude as actual morphological changes. Failing to acknowledge systematic errors in photogrammetric reconstruction can therefore lead to substantial errors in calculated volume changes, and the misinterpretation as to whether sedimentation or erosion has occurred (see also Figure 5). Additionally, the correct interpretation of temporal trends in sedimentation is important for the understanding of sediment fluxes between the reaches and potentially the forcing mechanisms of these fluxes. Note that the responses of reaches A and CD largely coincide (the latter is slightly damped) whereas without the registration adjustment a significant delay in the signal between these reaches could have been identified.

4. DISCUSSION

4.1 Bundle adjustment

Comparison of SfM and classical photogrammetric approaches to archival images of braided river reaches showed that the two methods resulted in no clear preference for either method in terms of the reprojection error or the mean control point RMSE from the bundle adjustment (Table 2). Values obtained were comparable to the theoretically-expected precision. When considering mean error, the residuals did suggest the presence of systematic error (Table 3). Closer inspection of the exterior orientation parameters showed that, in general, SfM and classical photogrammetric values were comparable (Table 4). Differences were largely attributed to the interaction between exterior orientation and lens parameter optimization during the SfM photogrammetric process. The interaction was mainly revealed in counterbalancing adjustments, where changes in estimated focal length were largely compensated by changes in the estimated flying height (Figure 2). However, for this

432 scaling relation to be completely valid the camera should be oriented vertically and the terrain horizontal (e.g. Gardner 1939); whereas the former is more or less the case in archival aerial photography, the latter is not the case in this study.

Closer assessment of the self-calibrated lens distortion using camera calibration certificates revealed no indication of excessive distortion which may be introduced to compensate for potential errors in the estimation of external orientation parameters. Indeed, we did not find the dome-like errors which have been earlier found to result from insufficiently modelled lens distortion in SfM photogrammetry using non-metric cameras (e.g. Javernick *et al.* 2014, Eltner and Schneider 2015). The polynomial form of the radial distortion could not be resolved, but this is not surprising for archival imagery. First, the stereo geometry of archival imagery, based on near-nadir corridor/grid mapping, was not designed for camera self-calibration which works better with convergent/rotated image configurations (Remondino and Fraser 2006; Wackrow and Chandler 2008; 2011; James and Robson 2014). Second, the metric cameras used in archival imagery have very little distortion, in comparison with consumer-grade close-range cameras that are often used with SfM, but also in comparison with the pixel resolution on which the self-calibration operates. More generally, self-calibration in SfM applications needs to be assessed with care where it is subject to internal correlation between the K terms (Fraser 1997), allowing for equifinal solutions (Carbonneau and Dietrich 2016), and may be subject to residual systematic error and noise in the dataset. Lens parameters should be considered as model-specific modelled and cannot be transferred to other applications or treated as universal values (e.g. Luhmann *et al.* 2014).

Thus considering the combined bundle adjustment and camera self-calibration, similar levels of optimization (e.g. RMSE) can be achieved with different combinations of exterior orientation and lens parameters, and that simultaneous unsupervised self-calibration and bundle adjustment does not necessarily recover the ‘correct’ lens parameters and hence the correct exterior orientation. These findings are relevant when using archival imagery, for which camera calibration certificates may not always be available (e.g. Aguilar *et al.* 2013), but the question remains whether it really matters for their application. Concerning focal length, others (e.g. Caduff and Rieke-Zapp, 2014) have identified the need for self-calibration in order to obtain a converged bundle adjustment. The fact that the changes in focal length and flying height with the SfM photogrammetric approach scaled linearly on one another (Figure 2) suggests that focal length optimization should not be a major concern unless it is attempting to correct for non-linear inaccuracies which may result from either measured (e.g. GCPs) or modelled parameters (e.g. lens distortion). Concerning lens distortion, we found no evidence for interaction with exterior parameters, although in this application with metric cameras there was also no real ‘incentive’ for such interaction. Fraser (1997) already established this coupling to be low. Error resulting from lens distortion in this type of archival application is only of secondary importance and of little influence on the overall error.

Bundle adjustment is a complex mathematical procedure, with a large number of degrees of freedom and many potential parameter correlations complicating the assessment of the influence of single parameters. In general, our findings emphasise the need for SfM applications to pay close attention to the bundle adjustment results, in relation to applied lens model optimization. They challenge the idea that SfM frees the user from the traditional concerns in photogrammetry and emphasise the importance of transparency in the algorithms used in SfM software packages (e.g.

Smith *et al.* 2015), as argued before in relation to early applications of automated digital photogrammetry (Chandler 1999; Lane *et al.* 2000).

4.2 Image properties and data quality

There was clear evidence that the success of a SfM approach was related to the way that image properties are exploited by computer vision techniques. The primary advantage with respect to the classical approach is the use of a much greater number of matched tie-points (Table 2) which are fully distributed over the images (not limited to the zone of interest), so, at least partly, overcoming the dependency on and limits imposed by GCP availability for archival purposes (e.g. James *et al.* 2006; Walstra *et al.* 2011). The addition of large amounts of automatically generated tie-points, where their accuracy is limited to simple outlier detection, to a small number of accurate, user-specified GCP's provides a good constraint for bundle adjustment. Not only are SfM methods efficient in the unsupervised automatic aligning of the photographs, we have also found that they lead to a more accurate alignment based on the limited required registration adjustment in the yaw (K) orientation (Figure 7).

Image texture, which can be effectively quantified using a simple measure of spectral entropy (Laliberte and Rango 2009), directly impacts the number of generated tie-points in bundle adjustment and subsequent reprojection error and RMSE (Figure 4). This is in line with the general notion that the texture is of critical importance for SfM feature extraction (e.g. Westoby *et al.* 2012). Where the texture of archival images is predefined, the entropy may be used for quality screening of photographs. This however only indicates a potential, where spatial variability, in the form of surface cover and general morphology, is also required for feature extraction. For the successful matching of extracted features, high image overlap between photographs is also important (Figure 4; e.g. Westoby *et al.* 2012). This enables the redundance of tie-points and prevents potential difficulties in feature matching, due to dissimilarities between images that arise from perspective changes, which in turn allow for a reduced error in bundle adjustment. Here, a possible constraint on the application of SfM based archival photogrammetry arises where image acquisition in classical photogrammetry is designed with relatively limited overlap. This is however with reason, where from classical photogrammetry we know that the accuracy of elevation change actually increases with increasing perspective changes due to the parallax shift, which indicates a potential optimum in overlap/perspective change when applying SfM photogrammetry. Another difference arises where SfM algorithms extensively use tie-points and their automatic extraction and matching is scale invariant (Figure 4). SfM algorithms are therefore less dependent on image scale as compared to classical photogrammetry, which relies more strongly on GCP identification which is scale dependent.

Limitations in available image quality (texture), image overlap and image configuration (near-nadir imagery) in archival imagery, in combination with the interaction between bundle adjustment and camera self-calibration demand the utmost insight and control in SfM photogrammetry. Where photogrammetric techniques will further develop and (hopefully) manifest themselves in SfM software, image acquisition properties are predefined and may be assessed for their SfM photogrammetric potential, just like the typically applied image scale. The ample use of GCPs may constrain the bundle adjustment and suppress errors (e.g. Eltner and Schneider 2015). In archival applications these are likely to be limited, but in any case it is advisable to exploit these to the fullest in bundle adjustment control and preferably not as check points where error may also be estimated through subsequent registration or GCP sensitivity analysis. Despite the limitations we demonstrated that SfM methods do not only have the potential for the application in archival photogrammetry (Gomez *et al.* 2015), they can be used for the accurate quantification of river-floodplain morphology. This is enhanced by the dense-matching/high resolution algorithms that these methods use which allow for higher precision and (associated) lower local error through interpolation in comparison with classical photogrammetry (e.g. Eltner *et al.* 2016).

4.3 Systematic error minimization

In all photogrammetric applications, regardless as to whether a SfM or classical approach is used, residual systematic errors may be expected which need to be independently verified both with other techniques or other data sets (Fonstad *et al.* 2013; Eltner *et al.* 2016). We have shown that this may not always be apparent from bundle adjustment quality parameters (mean error, Table 2), but may be revealed through registering the photogrammetrically derived point clouds to a lidar-based reference grid (for example Figure 5). We found systematic errors on the reach scale that were typically of the order of decimeters (Table 5). After registration adjustment the residual error values were of the order of centimeters, and with two exceptions all values were within 15 cm. The effectiveness of the adjustment, in the form of the relative decrease in bias, varied somewhat amongst reaches and between years.

Closer inspection of the applied registration adjustment, orientation and magnitude, revealed both consistencies amongst the reaches, giving confidence in the adjustment to correct for systematic error, as well as considerable differences, which may indicate that errors are complex/non-linear and potentially noise dominated (Figure 7). The effectiveness of the registration also varied with the magnitude of the required change in orientation parameters, where it must be noted that the adjustment may also, theoretically, introduce an additional error. The required reduction in the (linear) systematic error was of the same order of magnitude or smaller than the differences we found between SfM and classical approaches. From this we can conclude that potential limitations associated with the application of SfM algorithms in the form of linear error (e.g. through focal length modelling) may be overcome through subsequent registration. Indeed, registration adjustments are relevant for all photogrammetric applications, SfM or classical, where systematic linear errors may originate from the propagation of random error in the external orientation parameters (Westaway *et al.* 2003; Lane *et al.* 2004).

Failing to acknowledge systematic errors in photogrammetrically derived point clouds will allow them to translate and potentially amplify when determining morphological change. As we have shown in Figure 8, this may lead to the misinterpretation of the occurrence of erosion/sedimentation, the absolute quantities of change and morphologic variability in time (in our case the decadal scale) and space (in our case between reaches). The application of archival photogrammetry in low relief environments such as river-floodplain systems is particularly sensitive to such errors (e.g. Heritage *et al.* 1998; Lane *et al.* 2010). Note that when no independent, high resolution reference dataset is available, a photogrammetrically derived DEM (typically the most recent) may be sufficient for the analysis of (relative) morphological change. Registration not only provides a means for minimizing linear structural errors, but also provides an uncertainty estimation for residual non-linear structural and random error (this may be conservative where particularly on the longer term zones may not be entirely stable due to e.g. slope processes, vegetation growth) for the assessment of detection limits and error propagation in elevational and volumetric changes (Lane *et al.* 2004). Finally the registration procedure provides general insight into the quality of the photogrammetric reconstruction.

5. CONCLUSIONS

In this study we applied computer vision based SfM methods to archival imagery for the quantification of river and floodplain morphology. Besides the widely recognized efficiency and precision, we found the resulting quality may be comparable to that obtained with classical methods. We showed that this application requires the careful consideration of photogrammetric principles to avoid and to mitigate structural error in DEMs. These may heavily impact the interpretation of morphological change, particularly for the application of archival photogrammetry in low relief river-floodplain environments. The results from this study may be summarised along three phases of the photogrammetric process, namely image acquisition, bundle adjustment and point cloud registration:

The potential of the application of SfM photogrammetric methods to archival imagery can be evaluated by reference to: (1) the temporal frequency and scale of images in relation to the relief that is to be measured and the magnitude of expected changes; in this sense SfM does not differ from the classical application; (2) image texture, which can be quantified using entropy, controls the extent to which computer vision techniques can detect and match tie-points (3) image overlap and configuration, which enables the redundance of tie-points and enhances their accuracy (less mismatching). These last two points specifically apply to SfM photogrammetry where the tie-points largely control bundle adjustment precision, particularly with respect to the alignment of images; 4) GCP's are ideally included in bundle adjustment as a basis on which the SfM computer vision techniques can enhance the dataset on which bundle adjustment is based and thereby it's potential quality.

Despite non-ideal archival image acquisition, near-nadir and limited overlap which affect camera self-calibration and bundle adjustment, the bundle adjustment quality we acquired with SfM was similar to that which was acquired using classical photogrammetry. In both cases the quality of the photogrammetric reconstruction requires SfM software to provide insight and control over bundle adjustment parameters. Interaction between lens modelling parameters and exterior orientation parameters needs to be assessed in relation to one another. We found (linear) interaction between focal length and flying altitude, but these largely compensated each other. We did not find any indication that non-linear or dome-like errors were introduced through camera self-calibration, neither in the DEMs nor in the modelled distortion.

Registration adjustment provides a means for addressing linear systematic error in point clouds that remains, even with reliable bundle adjustment results, through: (1) systematic error detection which may be the result of (random) error propagation in classical or SfM photogrammetry; (2) error minimization through registration, which was able to compensate the potential (additional) error associated with the application of SfM photogrammetry, preventing error propagation into volume changes; and (3) quality assessment of the bundle adjustment and point cloud, which was possible through quantifying the residual error and analyzing the required rotation/translation.

ACKNOWLEDGEMENTS

Maarten Bakker is supported by the Swiss National Science Foundation, Synergia grant CRSII2_147689, awarded to Fritz Schlunegger, Stéphanie Girardclos, Stuart Lane, Jean-Luc Loizeau and Peter Molnar. SwissTopo provided the scanned aerial photographs and Natan Micheletti provided the GCP data used in the study. Additional support came from the Canton Valais, the Fondation Herbette and the Commune of Evolène. We would like to thank Anette Eltner, an anonymous reviewer and Editor Mike Kirkby for their detailed and constructive comments which have led to the improvement of this manuscript.

REFERENCES

Aguilar, M.A., Aguilar, F.J., Fernández, I., Mills, J.P. 2013. Accuracy assessment of commercial self-calibrating bundle adjustment routines applied to archival aerial photography. The Photogrammetric Record 28(141): 96-114. DOI: 10.1111/j.1477-9730.2012.00704.x.

Barker, R., Dixon, L., Hooke, J. 1997. Use of terrestrial photogrammetry for monitoring and measuring bank erosion. Earth Surface Processes and Landforms 22(13): 1217-1227. DOI: 10.1002/(SICI)1096-9837(199724)22:13<1217::AID-ESP819>3.0.CO;2-U.

Bertin, S., Friedrich, H., Delmas, P., Chan, E., Gimel'farb, G. 2015. Digital stereo photogrammetry for grain-scale monitoring of fluvial surfaces: Error evaluation and workflow optimisation. ISPRS Journal of Photogrammetry and Remote Sensing 101: 193-208. DOI: 10.1016/j.isprsjprs.2014.12.019.

Bezinge, A., Clark, M., Gurnell, A., Warburton, J. 1989. The management of sediment transported by glacial melt -water streams and its significance for the estimation of sediment yield. Annals of Glaciology 13: 1-5.

Brasington, J., Langham, J., Rumsby, B. 2003. Methodological sensitivity of morphometric estimates of coarse fluvial sediment transport. Geomorphology 53(3–4): 299-316. DOI: 10.1016/S0169-555X(02)00320-3.

Brown, D.C. 1971. Close-range camera calibration. Photogrammetric engineering 37(8): 855-866.

Caduff, R., Rieke-Zapp, D. 2014. Registration and visualisation of deformation maps from terrestrial radar interferometry using photogrammetry and Structure from Motion. The Photogrammetric Record 29(146): 167-186. DOI: 10.1111/phor.12058.

Carbonneau, P.E., Dietrich, J.T. 2016. Cost-effective non-metric photogrammetry from consumer-grade sUAS: implications for direct georeferencing of structure from motion photogrammetry. Earth Surface Processes and Landforms: n/a-n/a. DOI: 10.1002/esp.4012.

Castillo, C., Taguas, E.V., Zarco-Tejada, P., James, M.R., Gómez, J.A. 2014. The normalized topographic method: an automated procedure for gully mapping using GIS. Earth Surface Processes and Landforms 39(15): 2002-2015. DOI: 10.1002/esp.3595.

Chandler, J. 1999. Effective application of automated digital photogrammetry for geomorphological research. Earth Surface Processes and Landforms 24(1): 51-64. DOI: 10.1002/(SICI)1096-9837(199901)24:1<51::AID-ESP948>3.0.CO;2-H.

Chandler, J., Ashmore, P., Paola, C., Gooch, M., Varkaris, F. 2002. Monitoring river-channel change using terrestrial oblique digital imagery and automated digital photogrammetry. Annals of the Association of American Geographers 92(4): 631-644.

Chandler, J., Moore, R. 1989. Analytical photogrammetry: a method for monitoring slope instability. Quarterly Journal of Engineering Geology and Hydrogeology 22(2): 97-110.

De Rose, R.C., Basher, L.R. 2011. Measurement of river bank and cliff erosion from sequential LIDAR and historical aerial photography. Geomorphology 126(1–2): 132-147. DOI: 10.1016/j.geomorph.2010.10.037.

Dietrich, J.T. 2016. Riverscape mapping with helicopter-based Structure-from-Motion photogrammetry. Geomorphology 252: 144-157. DOI: 10.1016/j.geomorph.2015.05.008.

Eltner, A., Baumgart, P., Maas, H.-G., Faust, D. 2015. Multi-temporal UAV data for automatic measurement of rill and interrill erosion on loess soil. Earth Surface Processes and Landforms 40(6): 741-755. DOI: 10.1002/esp.3673.

Eltner, A., Kaiser, A., Carlos, C., Rock, G., Neugirg, F., Abellan, A. 2016. Image-based surface reconstruction in geomorphometry - merits, limits and developments of a promising tool for geoscientists. Earth Surface Dynamics Discussions 3: 359–389. DOI: 10.5194/esurf-4-359-2016.

Eltner, A., Schneider, D. 2015. Analysis of different methods for 3d reconstruction of natural surfaces from parallel-axes uav images. The Photogrammetric Record 30(151): 279-299. DOI: 10.1111/phor.12115.

ERDAS Imagine 2009. LPS Project Manager User’s Guide: 454.

Fonstad, M.A., Dietrich, J.T., Courville, B.C., Jensen, J.L., Carbonneau, P.E. 2013. Topographic structure from motion: a new development in photogrammetric measurement. Earth Surface Processes and Landforms 38(4): 421-430. DOI: 10.1002/esp.3366.

Fraser, C.S. 1997. Digital camera self-calibration. ISPRS Journal of Photogrammetry and Remote Sensing 52(4): 149-159. DOI: 10.1016/S0924-2716(97)00005-1.

Gabbud, C., Micheletti, N., Lane, S.N. 2015. Lidar measurement of surface melt for a temperate Alpine glacier at the seasonal and hourly scales. Journal of Glaciology 61(229): 963-974. DOI: 10.3189/2015JoG14J226.

Gardner, I.C. 1939. Relation of camera error to photogrammetric mapping, Journal of Research of the National Bureau of Standards 22 (RP1177): 209-238.

Gilvear, D., Bryant, R. 2005. Analysis of aerial photography and other remotely sensed data. In Tools in Fluvial Geomorphology. Kondolf, G.M.,Piégay, H. (eds), John Wiley & Sons, Ltd: 135-170.

Gilvear, D.J., Waters, T.M., Milner, A.M. 1995. Image analysis of aerial photography to quantify changes in channel morphology and instream habitat following placer mining in interior Alaska. Freshwater Biology 34(2): 389-398. DOI: 10.1111/j.1365-2427.1995.tb00897.x.

Gomez, C., Hayakawa, Y., Obanawa, H. 2015. A study of Japanese landscapes using structure from motion derived DSMs and DEMs based on historical aerial photographs: New opportunities for vegetation monitoring and diachronic geomorphology. Geomorphology 242: 11-20. DOI: 10.1016/j.geomorph.2015.02.021.

Gonzalez, R.C., Woods, R.E., Eddins, S.L. 2003. Digital image processing using MATLAB. New Jersey, Prentice Hall: 609.

Gurnell, A. 1983. Downstream channel adjustments in response to water abstraction for hydro-electric power generation from alpine glacial melt-water streams. The Geographical Journal 149(3): 342-354. DOI: 10.2307/634009.

Habib, A., Ghanma, M., Kima, C., Mitishita, E. 2004. Alternative approaches for utilizing lidar data as a source of control information for photogrammetric models. International Archives of Photogrammetry, Remote Sensing and Spatial Information Sciences, 35 (Part B1) B1: 193–198.

Heritage, G., Hetherington, D. 2007. Towards a protocol for laser scanning in fluvial geomorphology. Earth Surface Processes and Landforms 32(1): 66-74. DOI: 10.1002/esp.1375.

Heritage, G.L., Fuller, I.C., Charlton, M.E., Brewer, P.A., Passmore, D.P. 1998. CDW photogrammetry of low relief fluvial features: accuracy and implications for reach-scale sediment budgeting. Earth Surface Processes and Landforms 23(13): 1219-1233. DOI: 10.1002/(SICI)1096-9837(199812)23:13<1219::AID-ESP927>3.0.CO;2-R.

Heritage, G.L., Milan, D.J., Large, A.R.G., Fuller, I.C. 2009. Influence of survey strategy and interpolation model on DEM quality. Geomorphology 112(3–4): 334-344. DOI: 10.1016/j.geomorph.2009.06.024.

Honkavaara , E., Eskelinen, M.A., Pölönen, I., Saari, H., Ojanen, H., Mannila, R., Holmlund, C., Hakala, T., Litkey, P., Rosnell, T., Viljanen, N., Pulkkanen, M., 2016. Remote sensing of 3-D geometry and surface moisture of a peat production area using hyperspectral frame cameras in visible to short-wave infrared spectral ranges onboard a small Unmanned Airborne Vehicle (UAV). IEEE Transactions on Geoscience and Remote Sensing, 54 (9). DOI:10.1109/TGRS.2016.2565471.

James, M.R., Robson, S. 2012. Straightforward reconstruction of 3D surfaces and topography with a camera: Accuracy and geoscience application. Journal of Geophysical Research: Earth Surface 117(F3). DOI: 10.1029/2011JF002289.

James, M.R., Robson, S. 2014. Mitigating systematic error in topographic models derived from UAV and ground-based image networks. Earth Surface Processes and Landforms 39(10): 1413-1420. DOI: 10.1002/esp.3609.

James, T.D., Murray, T., Barrand, N.E., Barr, S.L. 2006. Extracting photogrammetric ground control from lidar DEMs for change detection. The Photogrammetric Record 21(116): 312-328. DOI: 10.1111/j.1477-9730.2006.00397.x.

Javernick, L., Brasington, J., Caruso, B. 2014. Modeling the topography of shallow braided rivers using Structure-from-Motion photogrammetry. Geomorphology 213: 166-182. DOI: 10.1016/j.geomorph.2014.01.006.

Kondolf, G.M., Larson, M. 1995. Historical channel analysis and its application to riparian and aquatic habitat restoration. Aquatic Conservation: Marine and Freshwater Ecosystems 5(2): 109-126. DOI: 10.1002/aqc.3270050204.

Küng, O., Strecha, C., Beyeler, A., Zufferey, J.-C., Floreano, D., Fua, P., Gervaix, F. 2011. The accuracy of automatic photogrammetric techniques on ultra-light UAV imagery. UAV-g 2011-Unmanned Aerial Vehicle in Geomatics.

Laliberte, A.S., Rango, A. 2009. Texture and scale in object-based analysis of subdecimeter resolution unmanned aerial vehicle (UAV) imagery. Geoscience and Remote Sensing, IEEE Transactions on Geoscience and Remote Sensing 47(3): 761-770. DOI: 10.1109/TGRS.2008.2009355.

Lane, S.N., Bakker, M., Gabbud, C., Micheletti, N., Saugy, J.-N. 2016. Sediment export, transient landscape response and catchment-scale connectivity following rapid climate warming and Alpine glacier recession. Geomorphology: 10.1016/j.geomorph.2016.1002.1015.

Lane, S.N, James, T., Crowell, M. 2000. Application of digital photogrammetry to complex topography for geomorphological research. The Photogrammetric Record 16(95): 793-821. DOI: 10.1111/0031-868X.00152.

Lane, S.N., Reid, S.C., Westaway, R.M., Hicks, D.M. 2004. Remotely sensed topographic data for river channel research: the identification, explanation and management of error. In Spatial modelling of the terrestrial environment. Kelly, R. E. J., Drake, N.A.,Barr, S.L. (eds), John Wiley & Sons, Ltd: 113-136.

Lane, S.N, Richards, K.S., Chandler, J.H 1993. Developments in photogrammetry; the geomorphological potential. Progress in Physical Geography 17(3): 306-328.

Lane, S.N., Richards, K.S., Chandler, J.H. 1994. Developments in monitoring and modelling small-scale river bed topography. Earth Surface Processes and Landforms 19(4): 349-368. DOI: 10.1002/esp.3290190406.

Lane, S.N., Westaway, R.M., Murray Hicks, D. 2003. Estimation of erosion and deposition volumes in a large, gravel-bed, braided river using synoptic remote sensing. Earth Surface Processes and Landforms 28(3): 249-271. DOI: 10.1002/esp.483.

Lane, S.N., Widdison, P.E., Thomas, R.E., Ashworth, P.J., Best, J.L., Lunt, I.A., Sambrook Smith, G.H., Simpson, C.J. 2010. Quantification of braided river channel change using archival digital image analysis. Earth Surface Processes and Landforms 35(8): 971-985. DOI: 10.1002/esp.2015.

Lowe, D. G. 2004. Distinctive image features from scale-invariant keypoints. International journal of computer vision 60(2): 91-110. DOI: 10.1023/B:VISI.0000029664.99615.94.

Luhmann, T., Robson, S., Kyle, S., Boehm, J., 2014. Close-Range Photogrammetry and 3D Imaging. Second edition. De Gruyter, Berlin, Germany: 683.

Micheletti, N., Lane, S.N., Chandler, J.H. 2015. Application of archival aerial photogrammetry to quantify climate forcing of alpine landscapes. The Photogrammetric Record 30(150): 143-165. DOI: 10.1111/phor.12099.

Miller, P., Mills, J., Edwards, S., Bryan, P., Marsh, S., Mitchell, H., Hobbs, P. 2008. A robust surface matching technique for coastal geohazard assessment and management. ISPRS Journal of Photogrammetry and Remote Sensing 63(5): 529-542. DOI: 10.1016/j.isprsjprs.2008.02.003.

Nebiker, S., Lack, N., Deuber, M. 2014. Building change detection from historical aerial photographs using dense image matching and object-based image analysis. Remote Sensing 6(9): 8310-8336. DOI: 10.3390/rs6098310.

Pasquale, N., Perona, P., Schneider, P., Shrestha, J., Wombacher, A., Burlando, P. 2011. Modern comprehensive approach to monitor the morphodynamic evolution of a restored river corridor. Hydrol. Earth Syst. Sci. 15(4): 1197-1212. DOI: 10.5194/hess-15-1197-2011.

Pérez Álvarez, J.A., Herrera, V.M., Martínez del Pozo, J.Á., de Tena, M.T. 2013. Multi-temporal archaeological analyses of alluvial landscapes using the photogrammetric restitution of historical flights: a case study of Medellin (Badajoz, Spain). Journal of Archaeological Science 40(1): 349-364. DOI: 10.1016/j.jas.2012.08.025.

Pix4D 2016. How are the internal and external camera parameters defined? Retrieved 25/04/2016, from https://support.pix4d.com/hc/en-us/articles/202559089#gsc.tab=0.

Pyle, C., Richards, K., Chandler, J. 1997. Digital photogrammetric monitoring of river bank erosion. The Photogrammetric Record 15(89): 753-764. DOI: 10.1111/0031-868X.00083.

Regamey, B. 2013. Télédétection des impacts à long terme de l'extraction de l'eau sur un système sédimentaire d'une vallée latérale alpine. Master's thesis in Geography, University of Lausanne. http://mesoscaphe.unil.ch/igul/doc.php?id=TIGL-859.pdf.

Remondino, F., Fraser, C. 2006. Digital camera calibration methods: considerations and comparisons. International Archives of Photogrammetry, Remote Sensing and Spatial Information Sciences 36(5): 266-272.

Riegl 2015. Riegl laser measurement systems: RiSCAN PRO version: 2.1.1. Horn, Austria.

Saint-Geours, N., Grelot, F., Bailly, J.S.,Lavergne, C. 2015. Ranking sources of uncertainty in flood damage modelling: a case study on the cost-benefit analysis of a flood mitigation project in the Orb Delta, France. Journal of Flood Risk Management 8(2): 161-176. DOI: 10.1111/jfr3.12068.

Sanyal, J., Lu, X.X. 2004. Application of remote sensing in flood management with special reference to monsoon asia: a review. Natural Hazards 33(2): 283-301. DOI: 10.1023/b:nhaz.0000037035.65105.95.

Seitz, S.M., Curless, B., Diebel, J., Scharstein, D., Szeliski, R. 2006. A comparison and evaluation of multi-view stereo reconstruction algorithms. 2006 IEEE Computer Society Conference on Computer Vision and Pattern Recognition (CVPR'06).

Smith, M. W., Carrivick, J.L.,Quincey, D.J. 2015. Structure from motion photogrammetry in physical geography. Progress in Physical Geography. DOI: 10.1177/0309133315615805.

Snavely, K.N. 2008. Scene Reconstruction and Visualization from Internet Photo Collections, University of Washington.

Stojic, M., Chandler, J., Ashmore, P., Luce, J. 1998. The assessment of sediment transport rates by automated digital photogrammetry. Photogrammetric Engineering and Remote Sensing 64(5): 387-395.

Strecha, C., Bronstein, A.M., Bronstein, M.M., Fua, P. 2012. LDAHash: Improved matching with smaller descriptors. Pattern Analysis and Machine Intelligence, IEEE Transactions on 34(1): 66-78.

Triggs, B., McLauchlan, P.F., Hartley, R.I., Fitzgibbon, A.W. 1999. Bundle adjustment—a modern synthesis. In Vision algorithms: theory and practice. Triggs, B., Zisserman, A., Szeliski, R. (eds), Springer: 298-372.

Vallet, J., Panissod, F., Strecha, C., Tracol, M. (2011). Photogrammetric performance of an ultra light weight swinglet UAV. UAV-g 2011-Unmanned Aerial Vehicle in Geomatics.

Wackrow, R., Chandler, J. H., Bryan, P. 2007. Geometric consistency and stability of consumer-grade digital cameras for accurate spatial measurement. The Photogrammetric Record 22(118): 121-134. DOI: 10.1111/j.1477-9730.2007.00436.x.

Wackrow, R., Chandler, J.H., 2008. A convergent image conguration for DEM extraction that minimises the systematic eects caused by an inaccurate lens model. The Photogrammetric Record, 23(121): 6-18. DOI: 10.1111/j.1477-9730.2008.00467.x.

Walstra, J., Chandler, J.H., Dixon, N., Wackrow, R. 2011. Evaluation of the controls affecting the quality of spatial data derived from historical aerial photographs. Earth Surface Processes and Landforms 36(7): 853-863. DOI: 10.1002/esp.2111.

Westaway, R.M., Lane, S.N., Hicks, D.M. 2001. Remote sensing of clear-water, shallow, gravel-bed rivers using digital photogrammetry. Photogrammetric Engineering and Remote Sensing 67(11): 1271-1282.

Westaway, R.M., Lane, S.N., Hicks, D.M. 2003. Remote survey of large-scale braided, gravel-bed rivers using digital photogrammetry and image analysis. International Journal of Remote Sensing 24(4): 795-815. DOI: 10.1080/01431160110113070.

Westoby, M.J., Brasington, J., Glasser, N.F., Hambrey, M.J., Reynolds, J.M. 2012. 'Structure-from-Motion' photogrammetry: A low-cost, effective tool for geoscience applications. Geomorphology 179: 300-314. DOI: 10.1016/j.geomorph.2012.08.021.

Wheaton, J.M., Brasington, J., Darby, S.E., Kasprak, A., Sear, D., Vericat, D. 2013. Morphodynamic signatures of braiding mechanisms as expressed through change in sediment storage in a gravel-bed river. Journal of Geophysical Research: Earth Surface 118(2): 759-779. DOI: 10.1002/jgrf.20060.

Wheaton, J.M., Brasington, J., Darby, S.E., Sear, D. A. 2010. Accounting for uncertainty in DEMs from repeat topographic surveys: improved sediment budgets. Earth Surface Processes and Landforms 35(2): 136-156. DOI: 10.1002/esp.1886.

Zhang, Z. 1994. Iterative point matching for registration of free-form curves and surfaces. International journal of computer vision 13(2): 119-152. DOI: 10.1007/BF01427149.

TABLES

Year	Images	Scale [1 :x]	Resolution [µm]	Texture (entropy)	Overlap [%]
1959	10	23200	21	3.39	15%
1965	6	21200	21	2.52	13%
1977	8	19600	14	3.47	30%
1983	12	19600	14	3.52	22%
1988	9	20900	14	3.59	19%
1995	8	26800	14	3.42	21%
1999	6	27000	14	3.27	17%
2005	3	24700	14	3.21	12%

Table 1 Overview and characteristics of historical aerial photographs.

Year	Number of GCPs	Tie-points per image	Reprojection error [m]	Mean RMSE [m]
1959	15 (14)	8387 (9)	0.08 (0.11)	±0.34 (±0.39)
1965	19 (17)	4254 (15)	0.06 (0.02)	±0.45 (±0.24)
1977	19 (41)	9563 (0)	0.04 (0.05)	±0.20 (±0.30)
1983	23 (25)	9692 (21)	0.04 (0.02)	±0.23 (±0.36)
1988	22 (18)	10505 (26)	0.04 (0.14)	±0.21 (±0.37)
1995	25	8387	0.05	±0.32
1999	20	10261	0.06	±0.44
2005	21 (30)	6240 (21)	0.08 (0.02)	±0.38 (±0.23)

Table 2 SfM block bundle adjustment results with classical photogrammetric reference values derived from (Regamey 2013) shown in brackets.

Year	Theoretical precision [m]	Mean RMSE [m]	X [m] ME | STDEV	Y [m] ME | STDEV	Z [m] ME | STDEV
1959	±0.49	±0.34 (±0.39)	0.01 | 0.30	0.08 | 0.39	0.00 | 0.33
1965	±0.45	±0.45 (±0.24)	-0.06 | 0.41	-0.10 | 0.57	-0.04 | 0.37
1977	±0.27	±0.20 (±0.30)	-0.01 | 0.18	-0.01 | 0.20	0.00 | 0.20
1983	±0.27	±0.23 (±0.36)	0.00 | 0.19	0.00 | 0.28	-0.01 | 0.21
1988	±0.29	±0.21 (±0.37)	-0.02 | 0.20	-0.01 | 0.22	-0.01 | 0.21
1995	±0.38	±0.32	0.01 | 0.33	0.01 | 0.41	0.01 | 0.21
1999	±0.38	±0.44	0.01 | 0.37	-0.20 | 0.57	-0.12 | 0.33
2005	±0.35	±0.38 (±0.23)	0.01 | 0.40	-0.01 | 0.53	0.02 | 0.21

Table 3 Theoretical precision, mean RMSE and control point mean error (ME) and standard deviation of error (STDEV) in X, Y and Z direction. The RMSE values in brackets are derived from (Regamey 2013) and determined by the authors (1977) and are given as a reference.

Year	Position			Orientation		
	ΔX [m]	ΔY [m]	ΔZ [m]	ΔK [°] (ΔXY [m])	ΔΘ [°] (ΔZ [m])	Φ [°] (ΔZ [m])
1959	-9.7	-0.9	-7.9	0.230 (2.01)	0.060 (0.52)	-0.062 (0.54)
1965	-2.2	2.6	-3.2	0.127 (1.11)	-0.005 (0.04)	-0.011 (0.10)
1977	1.1	2.3	-9.0	-0.322 (2.81)	-0.031 (0.27)	-0.065 (0.57)
1983	-2.9*	1.3*	-12.8	0.002 (0.02)	0.037 (0.32)	0.065 (0.57)
1988	-6.5	3.9	-0.3	-0.169 (1.47)	-0.016 (0.14)	0.001 (0.01)
1995	-3.2*	-1.6*				
1999	-2.8*	11.9*				
2005	-2.3*	-4.0*	28.0	-0.015 (0.13)	-0.373 (3.26)	-0.194 (1.69)
2005 fix	-3.5*	-4.5*	*6.4*	*-0.056 (0.49)*	*0.024* (0.21)	*-0.051* (0.45)

Table 4 Differences in exterior orientation parameters with respect to Regamey (2013) and Swisstopo. The maximum tilt adjustment (pitch or roll) has been translated to a potential error in meters. The 2005 fix row describes the 2005 bundle adjustment with fixed lens parameters.*

Year	ΔZ Reach A [m] before | after (change)	ΔZ Reach B [m] before | after (change)	ΔZ Reach CD [m] before | after (change)
1959	0.40 | 0.08 (0.32)	0.63 | 0.12 (0.51)	0.32 | 0.28 (0.04)
1965	0.05 | 0.04 (0.01)	-0.23 | 0.04 (0.19)	-0.06 | 0.05 (0.01)
1977	0.12 | 0.05 (0.07)	0.21 | 0.11 (0.10)	0.15 | 0.02 (0.13)
1983	-0.13 | 0.05 (0.08)	0.14 | 0.14 (0.00)	0.26 | 0.23 (0.03)
1988	0.24 | 0.04 (0.20)	0.12 | 0.08 (0.04)	0.32 | 0.14 (0.18)
1995	0.39 | 0.05 (0.34)	0.56 | 0.14 (0.42)	-0.10 | 0.09 (0.01)
1999	0.45 | -0.01 (0.44)	-0.01 | 0.04 (-0.03)	0.17 | 0.06 (0.11)
2005	0.02 | -0.01 (0.01)	0.53 | 0.09 (0.44)	0.52 | 0.03 (0.49)

Table 5 Stable-zone mean error (excluding outliers) values during multi-station adjustment. Improvements larger than 0.20 m are marked in green.

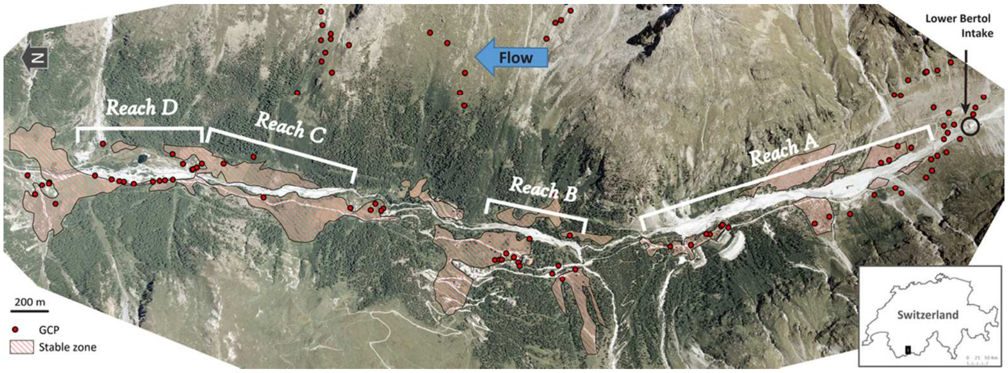

Figure 1 Orthoimage (2005) giving an overview of the sedimentation reaches in the Borgne d'Arolla River, Switzerland. GCPs and stable zones used for referencing and registration are shown.
Figure 1
104x38mm (300 x 300 DPI)

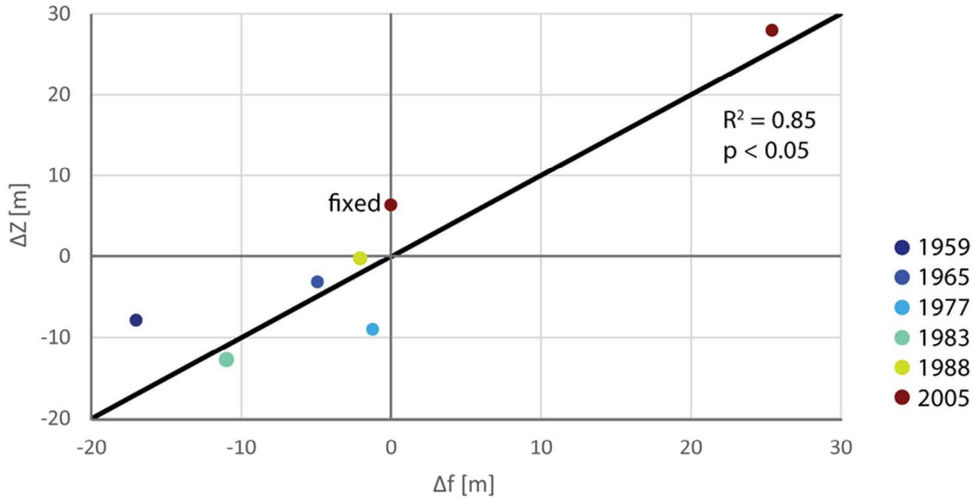

Figure 2 Relation between flying height difference (ΔZ) and the altitude difference that results from a change in focal length (Δf) with respect to the calibrated value. Note that the line and statistics, Pearson's R^2 and (significant) p value, follow a 1:1 relation and not a fitted regression line.
Figure 2
76x41mm (300 x 300 DPI)

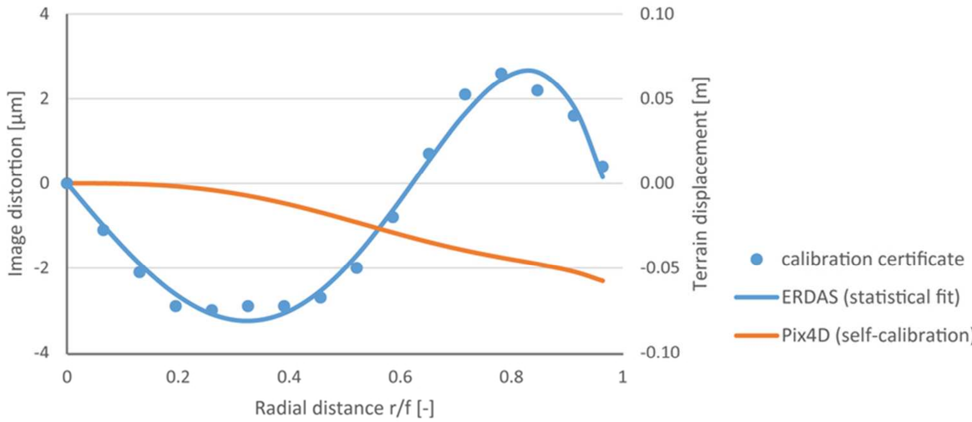

Figure 3 Radial distortion of the image and the related displacement in the terrain for the year with the largest calibrated distortion (2005). The ERDAS curve was statistically fitted using the measured deviations from the calibration certificate. The Pix4D curve was derived through self-calibration based on the images.
Figure 3
76x34mm (300 x 300 DPI)

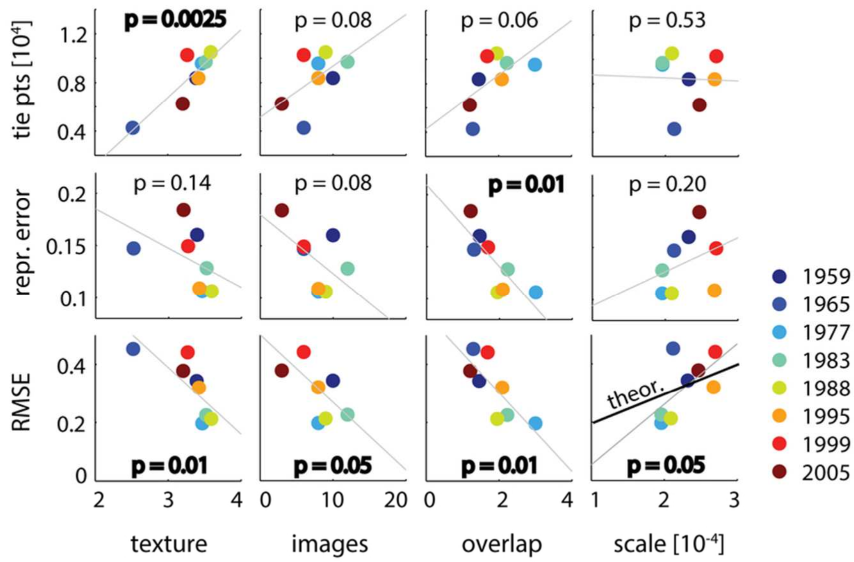

Figure 4 Scatter plots of image acquisition parameters, texture (entropy), images, image overlap and scale, vs. bundle adjustment parameters, tie points, reprojection error and RMSE. Plots include p values for Pearson's R linear correlation. Theoretical precision as a function of scale is plotted based on a 14 μm resolution (1959 and 1965 have a 21 μm resolution and therefore plot above the theoretical precision).
Figure 4
87x50mm (300 x 300 DPI)

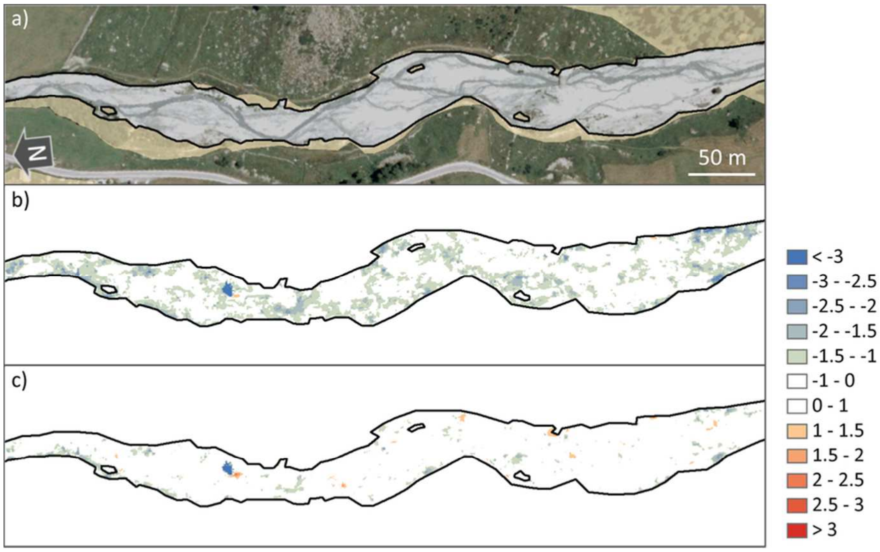

Figure 5 a) 2005 Orthoimage of the main section of reach C and stable zones (non-stable river flood plain and forested areas are shaded), b) 2005-2010 DoD before and c) after point cloud registration (blue is erosion, red is deposition). Limit of detection (95% certainty) is ~1m.
Figure 5
89x48mm (300 x 300 DPI)

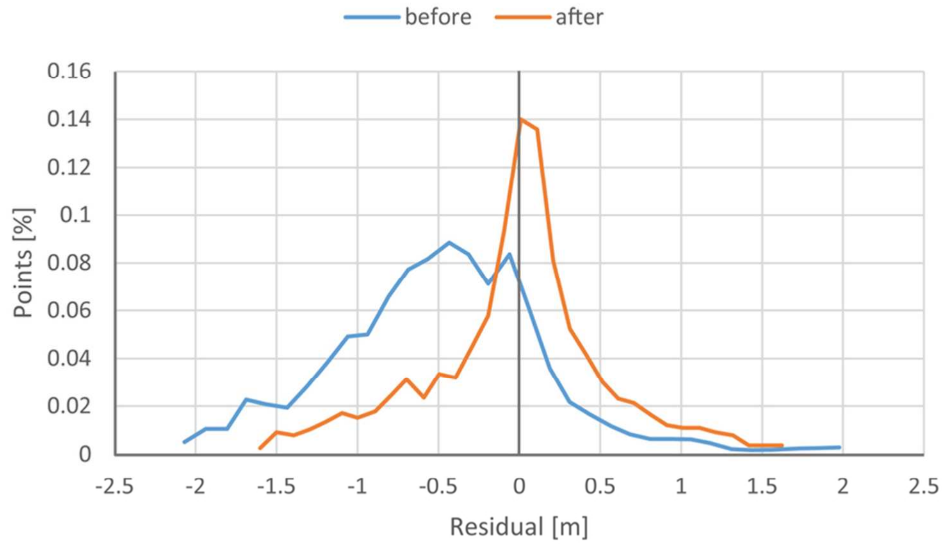

Figure 6 Normalised distribution of residual point distance between the stable zones in 2005 and 2010 for reach CD before and after registration.
Figure 6
76x45mm (300 x 300 DPI)

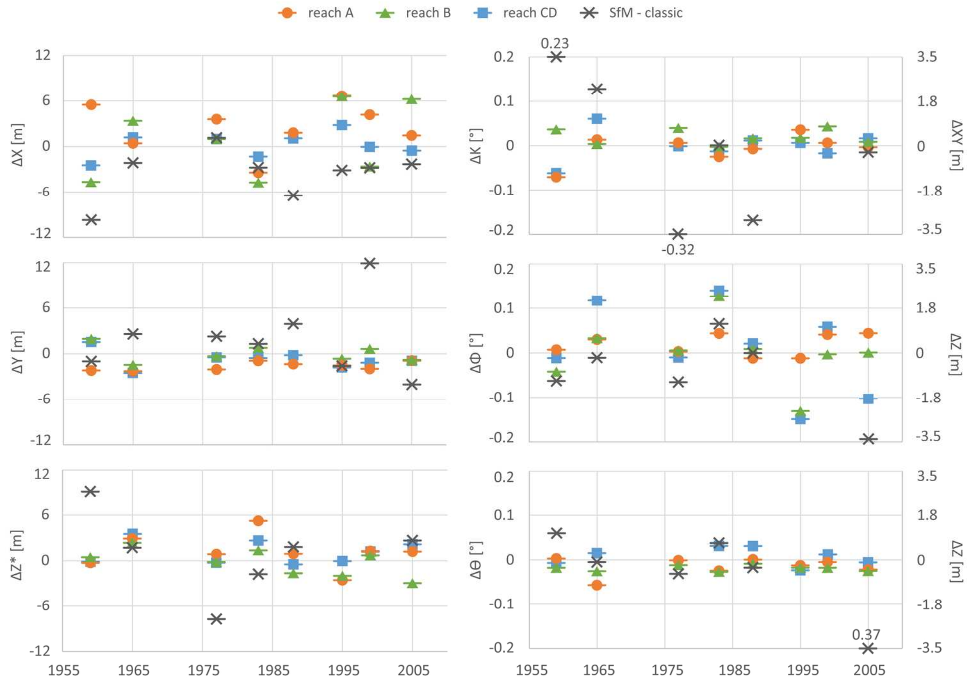

Figure 7 Adjustment of exterior parameters per reach with respect to deviation in bundle adjustment between SfM and classical photogrammetry (when they plot outside the y axis range, values are given - Table 4).*For ΔZ the values are corrected for focal length adjustment using the linear relation in Figure 2. The second y-axis for the orientation parameters gives the potential error in meters in a 1000 m reach.
Figure 7
186x132mm (300 x 300 DPI)

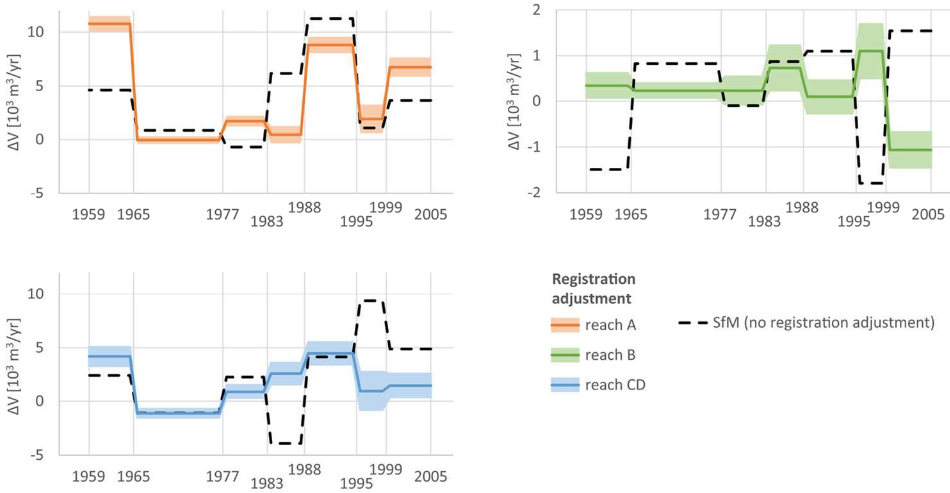

Figure 8 Average annual volume change per reach for periods between the available aerial photographs (specified on the x-axis). Change is displayed before registration adjustment (SfM) and after registration adjustment, including correction for residual stable-zone mean error (Table 5).The shaded uncertainty area for registration adjustment is based on a potential mean error in altitude values of ±0.05 cm for reach A and ±0.10 cm for reaches B and CD - these values were estimated based on Table 5.
Figure 8
127x64mm (300 x 300 DPI)